Neural Computing and Applications (2023) 35:9831–9840
https://doi.org/10.1007/s00521-023-08220-w

ORIGINAL ARTICLE

Data-driven Koopman fractional order PID control of a MEMS gyroscope using bat algorithm

Mehran Rahmani[1] · Sangram Redkar[1]

Received: 27 July 2022 / Accepted: 6 January 2023 / Published online: 24 January 2023

Abstract
Data-driven control methods are strong tools due to their predictions for controlling the systems with a nonlinear dynamic model. In this paper, the Koopman operator is used to linearize the nonlinear dynamic model. Generating the Koopman operator is the most important part of using the Koopman theory. Dynamic mode decomposition (DMD) is used to obtain eigenfunction for producing the Koopman operator. Then, a fractional order PID (FOPID) controller is applied to control the linearized dynamic model. A swarm intelligence bat optimization algorithm is utilized to tune the FOPID controller's parameters. Simulation results on micro-electromechanical systems (MEMS) gyroscope under conventional PID controller, FOPID, Koopman-based FOPID controller (Koopman-FOPID), and Koopman-FOPID control optimized by bat algorithm (Koopman-BAFOPID) show that the proposed Koopman-BAFOPID controller has better performance in comparison with three other controllers in terms of high tracking performance, low tracking error, and low control efforts.

Keywords Bat algorithm · Fractional PID control · Koopman operator · Dynamic mode decomposition · MEMS gyroscope · Data-driven method

1 Introduction

The MEMS gyroscope is an interesting device that can measure angular velocity by motion in x- and y-directions. This tool has been used in the automotive industry due to its low costs and small size [1, 2]. The control of the MEMS gyroscope is a difficult task because it constantly encounters external disturbances, which designing a suitable control method is required for this system [3].

An interesting area of study is data-driven control system, which uses data to control dynamical systems [4–6]. Several techniques are used to create data-driven structures such as deep neural network [7] and machine learning algorithms [8]. One effective method for linearizing the nonlinear dynamic model is the linear parameter varying (LPV) method. Hadian et al. [9] proposed a controller to reduce computation and conservatism for constrained nonlinear MIMO systems. Also, the simulation results verified the effectiveness of the proposed method in terms of disturbance rejection and high tracking performance. In addition, a model predictive controller (MPC) is proposed for nonlinear systems subjected to perturbations [10]. The LPV method is used to linearize the nonlinear dynamic model. Then, the MPC controller applied on the linearized model. The proposed method is robust against the disturbances. In data-driven control systems, Koopman theory is a strong approach. By projecting the system dynamics onto the Koopman eigenspace, Goswami and Paley [11] explore the issues of bilinearization and optimum control of a control-affine nonlinear system. Under certain assumptions, the suggested technique converts the dynamics into a bilinear system by using the Koopman canonical transform, especially the Koopman eigenfunctions of the drift vector field. Numerous examples of control-affine nonlinear systems are used to numerically demonstrate bilinearization and the best control strategy while assuming a quadratic cost function for the states and control input. The difficulties of making models that are subject to model-based control design methodologies make it challenging to

✉ Sangram Redkar
sangram.redkar@asu.edu

Mehran Rahmani
mrahma61@asu.edu

[1] The Polytechnic School, Ira Fulton School of Engineering, Arizona State University, Mesa, AZ 85212, USA

operate soft robots precisely. Koopman operator theory provides a framework for creating explicit dynamical models of soft robotics and controlling them with practiced model-based techniques [12]. How to derive the Koopman operator is the most crucial aspect of the Koopman theory, especially for complex systems with nonlinear dynamic system.

A useful approach for estimating the modes and eigenvalues of the Koopman operator is the DMD method. Utilizing an embedding into an infinite dimensional space, the Koopman operator offers a linear description of nonlinear systems. Among the most often used finite dimensional approximations of the Koopman operator are DMD and extended DMD [13, 14]. Koopman operator theory and the associated algorithm DMD were introduced by Ling et al. for the study and control of signalized traffic flow networks. They study DMD's application to various issues in signalized traffic as a model-free method for describing complicated oscillatory dynamics from observed data [15]. Wilches-Bernal et al. [16] propose a novel technique for identifying faults and other power quality issues. The major signal indicating a power quality event has occurred is identified by the suggested technique using the real component of the principal eigenvalue computed by the DMD. To discriminate between distinct failures, the study demonstrates how the suggested approach may be utilized to detect events utilizing current and voltage data. The performance of the strategy is examined in relation to the impact of the window size because the suggested method is window-based. To properly control the system, an appropriate controller can be used with the linearized DMD Koopman model such as linear quadratic regulator controller (LQR) [17] and model predictive controller (MPC) [18].

PID controller is a strong control method to control linear dynamic systems. It has been widely used in real-world systems due to its low cost and ease of implementation [19, 20]. By regulating the PID gains, it constantly evaluates errors and provides the best value. It is used to control different systems such as MEMS gyroscope [21], vehicle [22], and quadcopter [23]. However, the main drawbacks of the PID control method are that it's not robust control against the external disturbances. Although some useful methods can be used to tune the PID controller parameters such as axiomatic design theory based [24], the fractional control is also a suitable controller to improve the robustness and stability of PID controller. FOPID controller has been used in different research. Large uncertainty in dynamic and hydrodynamic properties as well as the signal transmission channel's time delay is the key challenges with autonomous underwater vehicles (AUV) motion control. For an AUV yaw control system, Liu et al. suggest a reliable FOPID controller architecture [25]. Erol [26] proposed a strong method of the pitch control system of large wind turbines with a FOPID controller that is delay dependent. The simulation findings demonstrate that outcomes for the delay margin are improved by using the proposed method. One of the main parts of FOPID controller design is how to tune the controller's gains to achieve the best performance. The bat optimization algorithm is a suitable method to tune the proposed controller's parameters.

The bat algorithm inspired by the echolocation behavior of microbats, with varying pulse rates of emission and loudness [27]. Finding solutions using algorithms based on population and local search is a benefit of employing the bat algorithm. We get both local rigorous exploitation and global variety from this combination, which is crucial for metaheuristic algorithms. The advantages of bat algorithm in comparison with particle swarm optimization and genetic algorithm are discussed in [28]. Based on the equivalent transfer function model and a reduced decoupler, the [29] describes a technique for developing independent FOPID controllers for two interacting conical tank-level processes. An optimization bat algorithm is used to increase the power system stability by tuning FOPID controller parameters [30].

This research paper proposes a new data-driven control algorithm to control the MEMS gyroscope. The contribution of this work is as follows:

1. The nonlinear dynamic model of the MEMS gyroscope is presented.
2. DMD method is used to generate eigenfunction and eigenvectors to obtain Koopman operator.
3. Using the Koopman theory, a FOPID controller is implemented to control the linearized dynamic model.
4. A bat metaheuristic optimization algorithm is used to tune the proposed control method parameters.
5. The robustness of the proposed control method verified by random noise application.

The rest of this paper is arranged as follows. Section 2 discusses the dynamic model of the MEMS gyroscope. Section 3 presents Koopman's theory. Section 4 describes the DMD method. Section 5 explains PID and FOPID control methods. Section 6 discusses the bat algorithm. Section 7 provides the simulation results. Section 7 demonstrates the conclusion.

2 Nonlinear dynamic model of MEMS gyroscope

An essential instrument for angular velocity measurement using x and y motion is the MEMS gyroscope [31–33]. This device has been used in automotive industry. A

typical z-axis MEMS gyroscope architecture is shown in Fig. 1.

A common MEMS gyroscope design includes sensor mechanisms, a proof mass suspended by springs, and an electrostatic actuation system for generating an oscillatory motion and determining the position and speed of the proof mass [34]. The proof mass is mounted on a frame that moves with a consistent linear velocity, while the gyroscope rotates at a gradually varying angular velocity, Ω_z. The centrifugal forces $m\Omega_z^2 x$ and $m\Omega_z^2 y$ are expected to be insignificant due to the modest displacements x and y. The development of the Coriolis forces, $2m\Omega_z^* \dot{y}$ and $2m\Omega_z^* \dot{x}$, is parallel to the driving and rotating axes [35]. The dynamics of the gyroscope are determined by the following equations.

$$m\,x + d_{xx}^* \dot{x} + d_{xy}^* \dot{y} + k_{xx}^* x + k_{xy}^* y + \beta x^3 = u_x^* + 2m\Omega_z^* \dot{y} \quad (1)$$

$$m\,y + d_{xy}^* \dot{y} + d_{yy}^* \dot{y} + k_{xy}^* x + k_{yy}^* y + \beta y^3 = u_y^* - 2m\Omega_z^* \dot{x} \quad (2)$$

The origin of the coordinates in Eqs. 1 and 2 is placed in the center of the proof mass since there is no external force applied on the system. The constants k_{xy}^* and d_{xy}^*, respectively, stand in for the asymmetric spring and damping coefficients. Despite the possibility of small unknown deviations from their nominal values, the control forces in the x- and y-direction, u_x^* and u_y^*, are usually accepted. There are also typical descriptions of the damping rates, d_{xx}^* and d_{yy}^*, and the spring constants of springs interacting in the x- and y-directions, k_{xx}^* and k_{yy}^*. Therefore, both electromechanical and mechanical nonlinearity, which is a positive constant, will introduce the terms βx^3 and βy^3. The following vector representation might be used to express Eqs. 1 and 2:

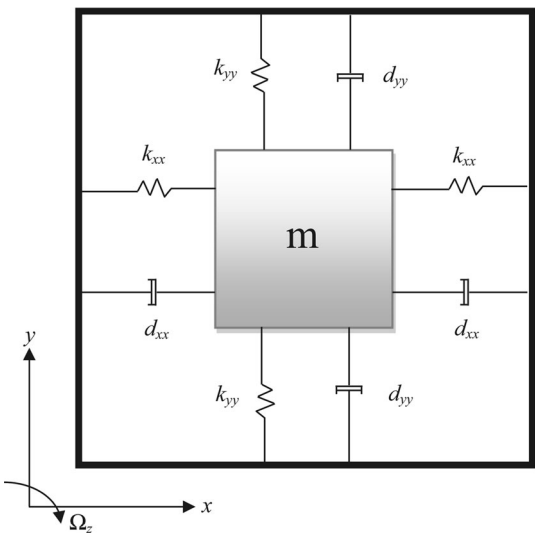

Fig. 1 MEMS gyroscope structure [22]

$$\frac{\ddot{q}}{q_0} + \frac{D^*}{m\omega_0}\frac{\dot{q}^*}{q_0} + \frac{K_a}{m\omega_0^2}\frac{q^*}{q_0} + \beta\frac{q^{*^3}}{q_0} = \frac{u^*}{m\omega_0^2 q_0} - 2\frac{\Omega^*}{\omega_0}\frac{\dot{q}^*}{q_0} \quad (3)$$

where $q^* = \begin{bmatrix} x^* \\ y^* \end{bmatrix}$, $u = \begin{bmatrix} u_x^* \\ u_y^* \end{bmatrix}$, $\Omega^* = \begin{bmatrix} 0 & -\Omega_z^* \\ \Omega_z^* & 0 \end{bmatrix}$, $D^* = \begin{bmatrix} d_{xx}^* & d_{xy}^* \\ d_{xy}^* & d_{yy}^* \end{bmatrix}$, $K_a = \begin{bmatrix} k_{xx}^* & k_{xy}^* \\ k_{xy}^* & k_{yy}^* \end{bmatrix}$, and nondimensional parameters as follows:

$$q = \frac{q^*}{q_0}\ d_{xy} = \frac{d_{xy}^*}{m\omega_0}\ \Omega_z = \frac{\Omega_z^*}{\omega_0} \quad (4)$$

$$u_x = \frac{u_x^*}{m\omega_0^2 q_0}\ u_y = \frac{u_y^*}{m\omega_0^2 q_0} \quad (5)$$

$$\omega_x = \sqrt{\frac{k_{xx}}{m\omega_0^2}}\ \omega_y = \sqrt{\frac{k_{yy}}{m\omega_0^2}}\ \omega_{xy} = \frac{k_{xy}}{m\omega_0^2} \quad (6)$$

where each axis' natural frequency is ω_0 and the reference length is q_0.

The following are the dynamic equations for the MEMS gyroscope.

$$q = -(D + 2\Omega)\dot{q} - K_b q - \beta q^3 + u + E \quad (7)$$

An external disturbance, E, might be modeled as:

$$q = -Y\dot{q} - Pq - \beta q^3 + u + E \quad (8)$$

where Y and P determine certain parameter variation uncertainties, $P = K_b$, and $Y = (D + 2\Omega)$. Therefore, Eq. (8) might be expressed as:

$$q = -(Y + \Delta Y)\dot{q} - (P + \Delta P)q - \beta q^3 + u + E \quad (9)$$

where. $q = \begin{bmatrix} x \\ y \end{bmatrix}$, $u = \begin{bmatrix} u_x \\ u_y \end{bmatrix}$, $\Omega = \begin{bmatrix} 0 & -\Omega_z \\ \Omega_z & 0 \end{bmatrix}$, $D = \begin{bmatrix} d_{xx} & d_{xy} \\ d_{xy} & d_{yy} \end{bmatrix}$, $K_b = \begin{bmatrix} \omega_x^2 & \omega_{xy} \\ \omega_{xy} & \omega_y^2 \end{bmatrix}$.

There are several ways to show Eq. (9):

$$q = -Y\dot{q} - Pq - \beta q^3 + u(t) + D(t) \quad (10)$$

D(t) describes as:

$$D(t) = -\Delta Y\dot{q} - \Delta P q + E \quad (11)$$

The expression for Eq. (10) in the x- and y- directions is

$$\begin{bmatrix} x \\ y \end{bmatrix} = -\left(\begin{bmatrix} d_{xx} & d_{xy} \\ d_{xy} & d_{yy} \end{bmatrix} + \begin{bmatrix} 0 & -2\Omega_z \\ 2\Omega_z & 0 \end{bmatrix}\right)\begin{bmatrix} \dot{x} \\ \dot{y} \end{bmatrix} - \begin{bmatrix} \omega_x^2 & \omega_{xy} \\ \omega_{xy} & \omega_y^2 \end{bmatrix}\begin{bmatrix} x \\ y \end{bmatrix} - \begin{bmatrix} \beta & 0 \\ 0 & \beta \end{bmatrix}\begin{bmatrix} x^3 \\ y^3 \end{bmatrix} + \begin{bmatrix} 1 & 0 \\ 0 & 1 \end{bmatrix}\begin{bmatrix} u_x \\ u_y \end{bmatrix} + \begin{bmatrix} D(t)_x \\ D(t)_y \end{bmatrix} \quad (12)$$

Equation (12) will be transformed into first-order dynamic equations by selecting the following parameters:

$$\begin{cases} x = z_1 \\ \dot{x} = z_2 \\ y = z_3 \\ \dot{y} = z_4 \end{cases}$$

Then, there is

$$\begin{cases} \dot{z}_1 = z_2 \\ \dot{z}_2 = -\omega_x^2 z_1 - \beta z_1^3 - d_{xx} z_2 - \omega_{xy} z_3 + (2\Omega_z - d_{xy}) z_4 + u_{z_1} + D_{z_1} \\ \dot{z}_3 = z_4 \\ \dot{z}_4 = -\omega_{xy} z_1 - (d_{xy} + 2\Omega_z) z_2 - \omega_y^2 z_3 - \beta z_3^3 - d_{yy} z_4 + u_{z_3} + D_{z_3} \end{cases} \tag{13}$$

Equation (13) shows

$$\dot{z} = A(z) + Bu \tag{14}$$

Equation (14) can be given in its classical form as follows:

$$\frac{d}{dt} z(t) = f(z) \tag{15}$$

3 Koopman theory

According to the Koopman operator theory, the crucial step to correctly a nonlinear dynamical system is to transform the nonlinear system's original form into an infinite dimensional state space so that the resulting system is linear [18].

The dynamic in discrete time defines as [36]:

$$z_{k+1} = F(z_k) \tag{16}$$

where F is characterized by

$$F(z(t_0)) = z(t_0) + \int_{t_0}^{t_0+t} f(z(\tau)) d\tau \tag{17}$$

When a finite-dimensional nonlinear system's dynamics are transferred to an infinite-dimensional function space using the Koopman operator theoretic method, the original system's dynamics becomes linear. g is a real-valued scalar measurement function and an observable, a part of an infinite-dimensional Hilbert space. The Koopman operator generates based on this observable as

$$\mathrm{Kg} = g \circ F \tag{18}$$

Smooth dynamics can be implemented using a continuous system.

$$\frac{d}{\mathrm{dt}} g(z) = \mathrm{Kg}(z) = \nabla g(z).f(z) \tag{19}$$

where the Koopman operator is K. Due to the infinite dimensions of the Koopman operator, which is significant but problematic for operation and representation. Instead of describing the development of all measurement functions in a Hilbert space, applied Koopman analysis approximates the evolution on a subspace covered by a small number of measurement functions. One can get a representation of the Koopman operator in a finite-dimensional matrix by limiting the operator to an invariant subspace. A Koopman invariant subspace is covered by any combination of the eigenfunctions of the Koopman operator [36]. When eigenvalue λ is satisfied by eigenfunction $\varphi(z)$ of the Koopman model.

$$\lambda\varphi(z) = \varphi(F(z)) \tag{20}$$

In continuous time, a Koopman eigenfunction $\varphi(z)$ is satisfied.

$$\frac{d}{\mathrm{dt}} \varphi(z) = \lambda\varphi(z) \tag{21}$$

A finite-dimensional approximation is required from the application side to approximate the Koopman operator. DMD method is one of the approaches that can estimate Koopman operator [36].

4 DMD method

A strong numerical method DMD utilizes to approximate Koopman operator.

$$Z' \approx AZ \tag{22}$$

where Z' is time shifted of matrix Z as:

$$Z = [z_1 \quad z_2 \quad \ldots\ldots]$$

The A can be found according to Eq. (22) as:

$$A = Z'Z^+ \tag{23}$$

where + represents the Moore–Penrose pseudoinverse. We may use singular value decomposition (SVD) on the snapshots to determine the dominating properties of the pseudoinverse of Z because a typical calculation involving A would need a significant amount of computation due to its huge n [37].

$$Z \approx U\Sigma V^* \tag{24}$$

where $U \in R^{n\times r}$, $\Sigma \in R^{r\times r}$, $V \in R^{n\times r}$, and * demonstrates the conjugate transpose. SVD's reduced rank for approximating Z is r. The eigenvectors can be defined as:

$$\phi = Z'V\Sigma^{-1}W \tag{25}$$

where W is eigenvectors of full rank system dynamic systems.

$$\phi = Z'V\Sigma^{-1}\boldsymbol{W} \tag{26}$$

Let λ be eigenfunction, then we will have:

$$KW = \lambda W \tag{27}$$

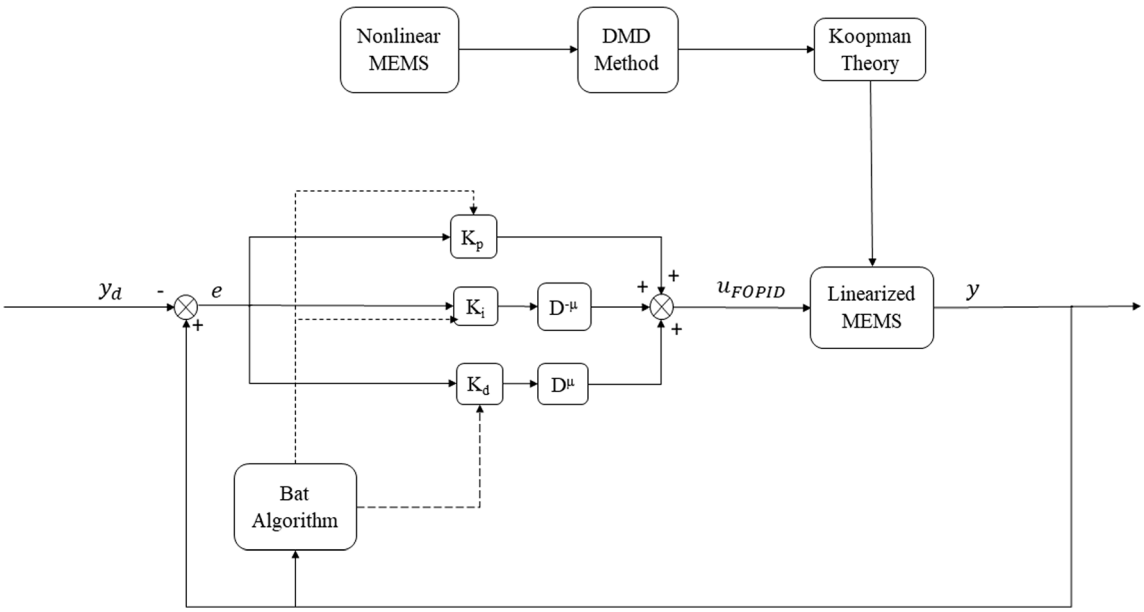

Fig. 2 The proposed control structure

where K is the Koopman operator.

The linearized dynamic model can be demonstrated as:

$$\frac{d}{\mathrm{dt}}y = Ky + Bu \tag{28}$$

5 FOPID control

PID controller is a suitable control method that has been used in many industrial applications [38–40]. It constantly evaluates the error by using its parameters K_p, K_i, and K_d and delivers the correct value. The PID controller can be defined as:

$$u_{\mathrm{PID}} = K_p e(t) + K_i \int_0^t e(\tau)d\tau + K_d \frac{\mathrm{de}(t)}{dt} \tag{29}$$

where $e(t) = y - y_d$, which y_d is desired trajectory.

The main problem of the PID controller is that it's not robust against external disturbances. Also, the stability of the PID controller is another issue that should be taken into consideration during the controller design.

Fractional control method introduced to improve the controller's performance. It can improve the stability and robustness of common PID controller. The FOPID controller can be defined as:

$$u_{\mathrm{FOPID}} = K_p e(t) + K_i D^{-\mu} e(t) + K_d D^{\mu} e(t) \tag{30}$$

where D is fractional operator defines as $D = \frac{d}{\mathrm{dt}}$ and μ is fractional order. The fractional type that we use in this research is Grunwald–Letnikov [41]. The Grunwald–Letnikov fractional derivative of the function $e(t)$ with respect to t is given

$$D_t^{\mu} e(t) = lim_{h \to 0} h^{-\mu} \sum_{k=0}^{n} (-1)^k \binom{\mu}{k} f(e(t) - kh) \tag{31}$$

where

$$\binom{\mu}{k} = \frac{\mu(\mu-1)(\mu-2)\ldots(\mu-k+1)}{k!} = \frac{\Gamma(\mu+1)}{k!\Gamma(\mu-k+1)}$$

The detailed explanation can be observed in [41]. The control structure shows in Fig. 2.

One of the main parts of FOPID controller design is how to tune the controller's parameters. The metaheuristic algorithms are the rich sources to tune the FOPID controller parameters.

6 Bat algorithm to tune the proposed controller parameters

The optimization technique known as the bat bio-inspired algorithm was influenced by how common bats use echolocation to find food. It is introduced in [27, 42] and used to resolve several optimization issues. The echolocation strategy of bats is used in the algorithm. These bats create an extremely loud sound pulse, and then, they listen for the echo that is returned from the nearby objects. Depending on the species, their signal bandwidth ranges change through harmonics. The i^{th} bat moves randomly at location x_i with velocity v_i and a set frequency f_{min}. To discover food, the bat changes its wavelength and volume.

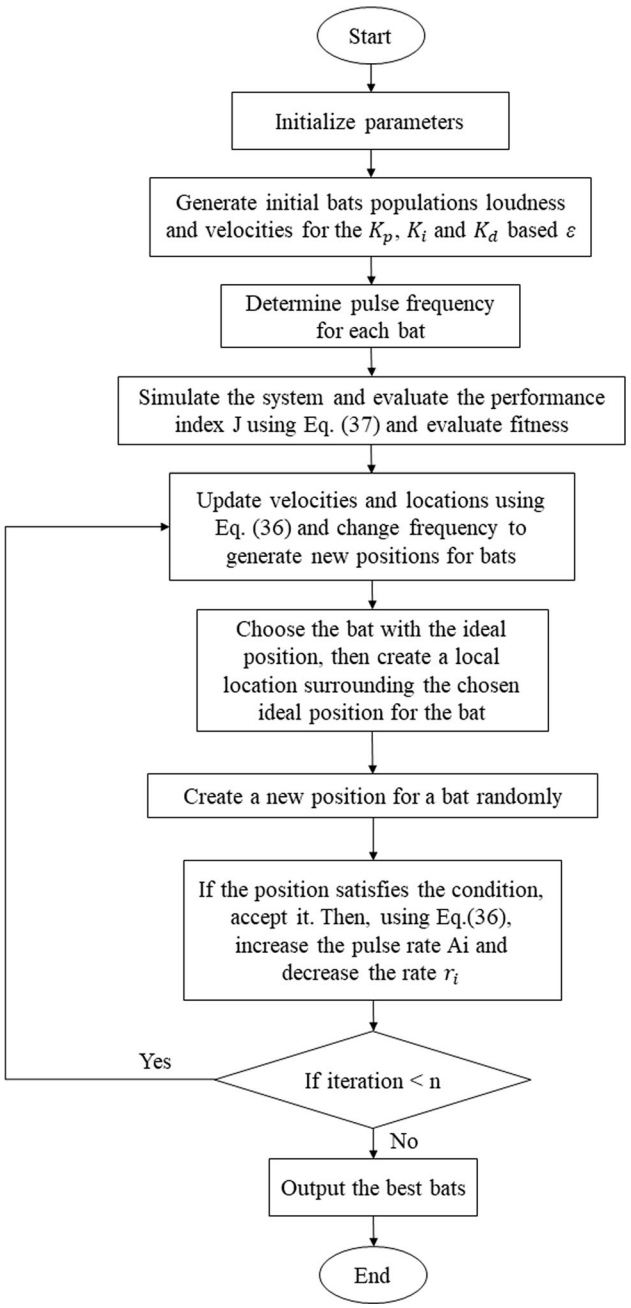

Fig. 3 Flow chart for a bat algorithm for tuning of Koopman-FOPID parameters

To improve the echolocation capabilities, objective function needs to be optimized. It is possible to develop an optimization algorithm from the way a bat searches for the best answer. The algorithms for bat-inspired echolocation can be created by enhancing certain of the microbats' echolocation characteristics. The features of bat echolocation are used to address an optimization issue brought about by the following hypotheses [43].

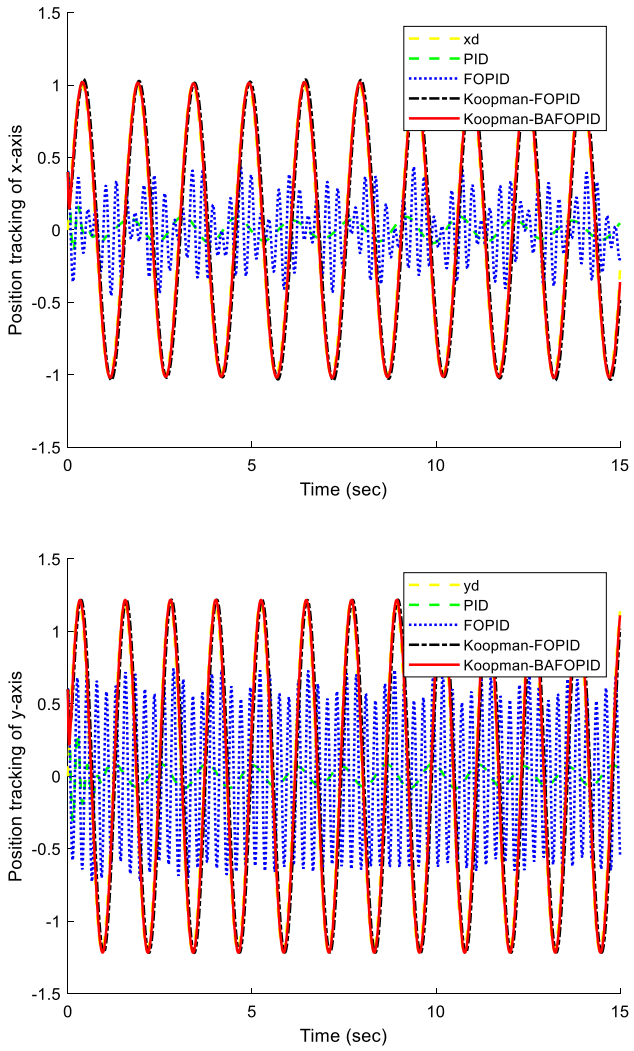

Fig. 4 Position tracking of x and y under the proposed controllers

1. Echolocation is a tool used by all bats to detect distance.
2. To locate prey, bats fly at random speeds of v_i at positions x_i with a fixed frequency and wavelength of $f_{\min}$ and a variable wavelength and frequency of A_0.
3. Depending on how close the prey is, they can control their wavelength/frequency and pulse emission rate, $r_i \in [0–1]$.
4. Their loudness decreases from high A_0 to low $A_{\min}$ levels as they get closer to the prey.

In real implementations, frequency occurs between [$f_{\min}$, $f_{\max}$] and is chosen to be similar to the size of the domain of interest. For a virtual bat to solve an optimization issue, rules must be developed to specify their locations and velocities in the d-dimensional search space. The following definitions apply to the new location x_i^+ and velocity v_i^+ at time step t [44].

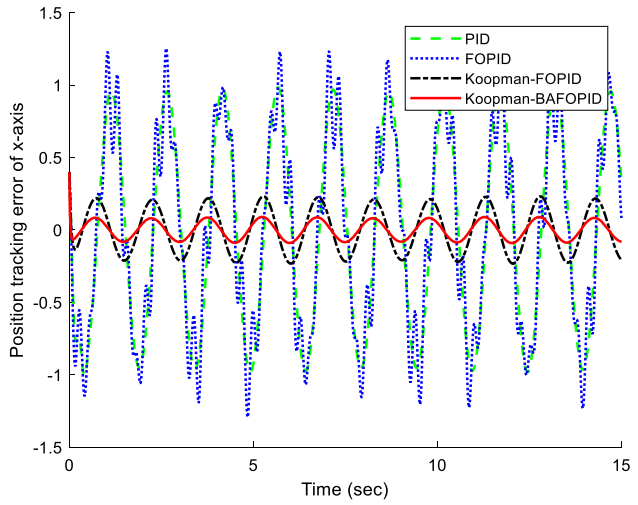

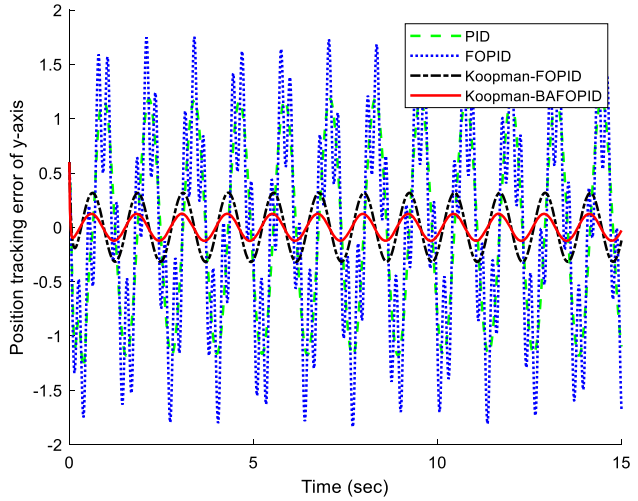

Fig. 5 Position tracking error of x- and y-directions under the proposed controllers

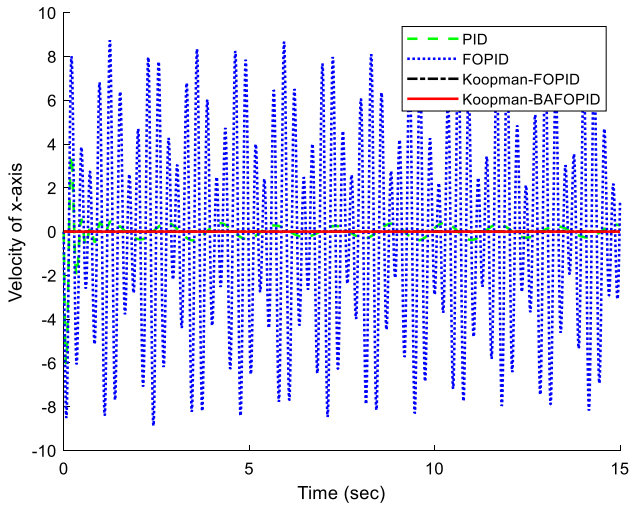

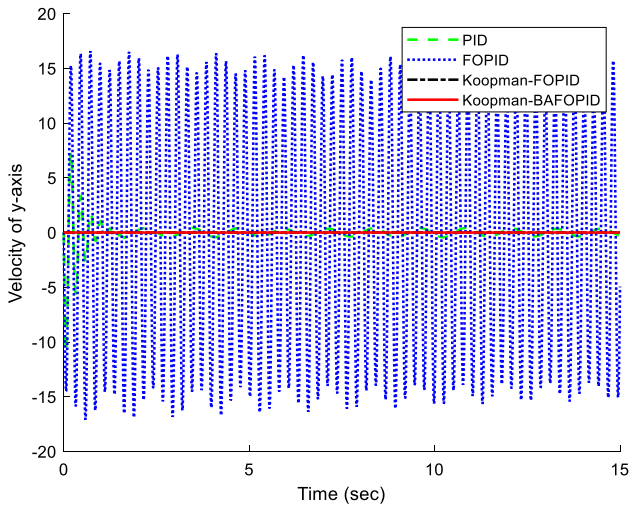

Fig. 6 Velocity of x- and y-directions under the proposed controllers

$$f_i = f_{\min} + (f_{\max} - f_{\min})\xi \tag{32}$$

$$v_i^t = v_i^{t-1} + \left(x_i^{t-1} - x^*\right)f_i \tag{33}$$

$$x_i^t = x_i^{t-1} + v_i^t \tag{34}$$

The current best solution across all N bats is represented by x^*, where $\xi \in [0–1]$ is the random vector generated at random from a uniform distribution. When a new solution is needed for local search, it is determined using the most recent bat loudness A_i and the most variance that can be tolerated max(var) at a time stop, as shown below.

$$x_{\text{new}} = x_{\text{old}} + \varepsilon A_i \max(\text{var}) \tag{35}$$

The volume drops and the pulse emission rate rises as a bat locates its prey. The bat is heading toward the best option, as shown by

$$A_i^{t+1} = \alpha A_i^t, r_i^{t+1} = r_r^{\circ}[1 - e^{-\gamma t}] \tag{36}$$

where α and γ are constant. Initial boundness is $A_i \in [0.1–0.9]$, initial emission rate is $r_0 \in [0–1]$, and $\alpha = \gamma = 0.9$. Bat algorithm is used for tuning the $[K_p, K_i, K_d]$ parameters of proposed controller for a MEMS gyroscope. This problem's objective function is described as follows [19]:

$$J = \int_0^{\infty} \left(w_1|e(t)| + w_2 u^2(t)\right)\mathrm{dt} + w_3 t_u \tag{37}$$

7 Simulation results

A MEMS gyroscope is controlled using the proposed Koopman-BAFOPID controller. Additionally, several comparative methods are used to show how effective the proposed bat algorithm is in adjusting the Koopman-FOPID parameters. The nonlinear dynamic equations of a MEMS gyroscope generated in this research. All simulations steps are simulated using MATLAB software. Figure 3 shows the flow chart of bat algorithm step in tuning

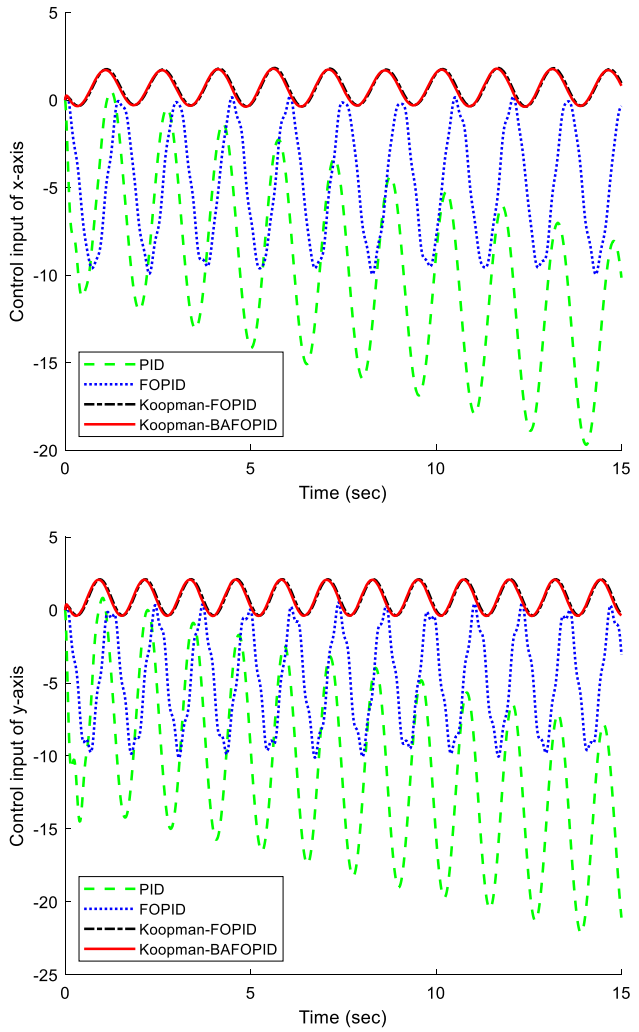

Fig. 7 Control efforts of *x*- and *y*-directions under the proposed controllers

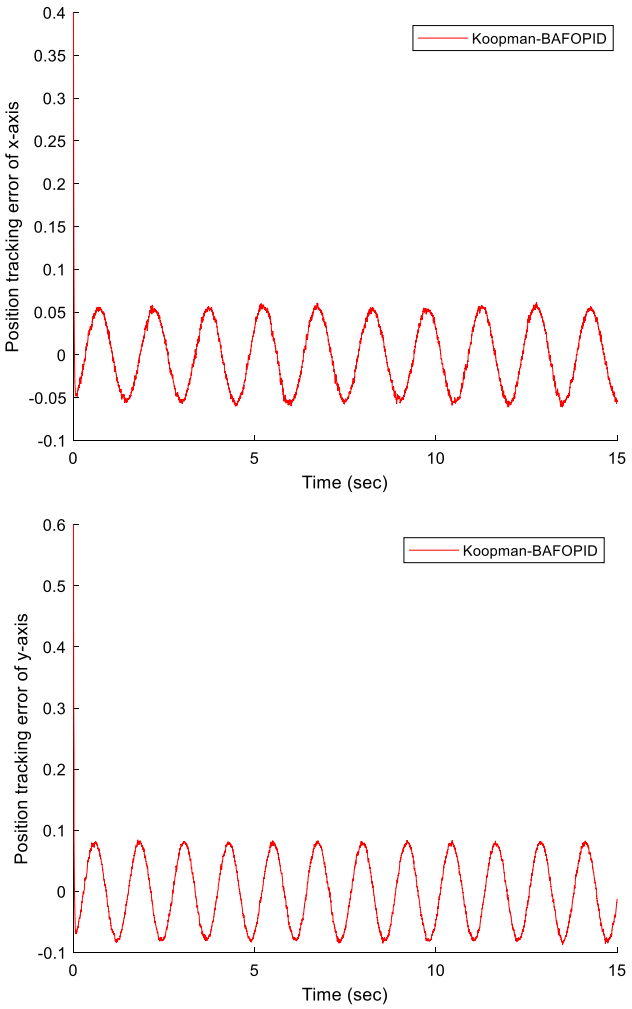

Fig. 8 Robustness of *x*- and *y*-directions under the proposed controllers

the Koopman-FOPID controller. The parameters of the proposed controller in this study are as follows: total population = 5; iteration = 20; loudness = 0.5; wavelength = 0.5; frequency $f_{\min} = 10$, $f_{\max} = 20$.

The objective function variables are set to $w_1 = 0.99$, $w_2 = 0.01$, and $w_3 = 2$. The tuned parameters of bat algorithm are $K_p = \text{diag}\{17.9901\}$, $K_i = \{22.3411\}$, and $K_d = \{27.2585\}$.

Figure 4 shows the trajectory tracking of x- and y-direction under PID, FOPID, Koopman-FOPID, and Koopman-BAFOPID controllers. It demonstrates that the proposed Koopman-BAFOPID controller has high tracking performance in comparison with the three other controllers. Figure 5 shows the position tracking error of x- and y-directions under PID, FOPID, Koopman-FOPID, and Koopman-BAFOPID controllers. It illustrates that the proposed Koopman-BAFOPID controller has low tracking error in comparison with the PID, FOPID, Koopman-FOPID, and Koopman-BAFOPID controllers. Figure 6 shows the velocity of x- and y-direction under PID, FOPID, Koopman-FOPID, and Koopman-BAFOPID controllers. A conventional PID controller applied on nonlinear MEMS gyroscope to control the x- and y-direction. The main problem of that controller is that it is not stable. Then, a FOPID controller used to remove the stability problem of conventional PID controllers. Figure 7 shows the control inputs under PID, FOPID, Koopman-FOPID, and Koopman-BAFOPID controllers. It demonstrates that the PID controller is not stable by increasing the control efforts when time is increased, but the FOPID controller fixed this problem. Therefore, using FOPID controller provides better stability along with using Koopman theory on nonlinear MEMS gyroscope. The robustness of the proposed control method is verified by random noise *0.5*randn(1,1) application. Figure 8 shows that the proposed control method is robust against the external disturbances.

8 Conclusion

This paper proposed a new Koopman-BAFOPID control of a nonlinear MEMS gyroscope. The PID controller stability improved by proposing FOPID controller. The Koopman theory used to drive a linear dynamic model of MEMS gyroscope. The DMD method used to estimate the Koopman operators numerically. Then, selected FOPID controller applied on linearized MEMS gyroscope dynamic model to control the x- and y-direction suitably. A bat algorithm implemented on Koopman-FOPID controller in order to tune the proposed controller parameters. The simulation results verified that the proposed Koopman-BAFOPID controller has better performance in comparison with PID, FOPID, and Koopman-FOPID controllers in terms high tracking performance, low tracking error, low control efforts, and high stability.

Funding Funding was provide by Directorate for Engineering, National Science Foundation.

Data Availability Data sharing is not applicable to this article as no datasets were generated or analyzed during the current study.

Declarations

Conflict of interest There are no conflicts of interest.

References

1. Solouk MR, Shojaeefard MH, Dahmardeh M (2019) Parametric topology optimization of a MEMS gyroscope for automotive applications. Mech Syst Signal Process 128:389–404
2. Classen, J., Frey, J., Kuhlmann, B., Ernst, P., & Bosch, R. (2007, August). MEMS gyroscopes for automotive applications. In *Advanced Microsystems for Automotive Applications* (pp. 291–306). Berlin, Germany: Springer.
3. Zhang WJ, Lin Y (2010) On the principle of design of resilient systems–application to enterprise information systems. Enterprise Information Systems 4(2):99–110
4. Gao S, Liu L, Wang H, Wang A (2022) Data-driven model-free resilient speed control of an Autonomous Surface Vehicle in the presence of actuator anomalies. ISA Transact 127:251
5. Xian B, Gu X, Pan X (2022) Data driven adaptive robust attitude control for a small size unmanned helicopter. Mech Syst Signal Process 177:109205
6. Liu H, Cheng Q, Xiao J, Hao L (2021) Data-driven adaptive integral terminal sliding mode control for uncertain SMA actuators with input saturation and prescribed performance. ISA Transact 128:624
7. Sun C, Dominguez-Caballero J, Ward R, Ayvar-Soberanis S, Curtis D (2022) Machining cycle time prediction: Data-driven modelling of machine tool feedrate behavior with neural networks. Robotics and Computer-Integrated Manufacturing 75:102293
8. Chen WH, You F (2021) Semiclosed greenhouse climate control under uncertainty via machine learning and data-driven robust model predictive control. IEEE Trans Control Syst Technol 30(3):1186–1197
9. Hadian M, Ramezani A, Zhang W (2022) An interpolation-based model predictive controller for input–output linear parameter varying systems. Inter J Dyn Cont 10:1–14
10. Hadian M, Ramezani A, Zhang W (2021) robust model predictive controller using recurrent neural networks for input-output linear parameter varying systems. Electronics 10(13):1557
11. Goswami D., and Paley DA (2021). Bilinearization, reachability, and optimal control of control-affine nonlinear systems: A Koopman spectral approach. IEEE Transact Automatic Cont
12. Bruder D, Fu X, Gillespie RB, Remy CD, Vasudevan R (2020) Data-driven control of soft robots using koopman operator theory. IEEE Trans Rob 37(3):948–961
13. Zanini F, Chiuso A (2021) Estimating Koopman operators for nonlinear dynamical systems: a nonparametric approach. IFAC-PapersOnLine 54(7):691–696
14. Jiang L, Liu N (2022) Correcting noisy dynamic mode decomposition with Kalman filters. J Comput Phys 461:111175
15. Ling E, Zheng, L, Ratliff LJ, & Coogan, S (2020). Koopman operator applications in signalized traffic systems. IEEE Transact Intell Transport Syst
16. Wilches-Bernal F, Reno MJ, Hernandez-Alvidrez J (2021) A Dynamic Mode Decomposition Scheme to Analyze Power Quality Events. IEEE Access 9:70775–70788
17. Mamakoukas G, Castano M, Tan X, & Murphey, T (2019). Local Koopman operators for data-driven control of robotic systems. In Robotics: Science and Systems.
18. Ping Z, Yin Z, Li X, Liu Y, Yang T (2021) Deep Koopman model predictive control for enhancing transient stability in power grids. Int J Robust Nonlinear Control 31(6):1964–1978
19. Rahmani M, Ghanbari A, Ettefagh MM (2016) Robust adaptive control of a bio-inspired robot manipulator using bat algorithm. Expert Syst Appl 56:164–176
20. Rahmani M, Komijani H, Ghanbari A, Ettefagh MM (2018) Optimal novel super-twisting PID sliding mode control of a MEMS gyroscope based on multi-objective bat algorithm. Microsyst Technol 24(6):2835–2846
21. Fei, J., & Chu, Y. (2016, August). Dynamic global PID sliding mode control for MEMS gyroscope using adaptive neural controller. In: 2016 joint 8th international conference on soft computing and intelligent systems (SCIS) and 17th international symposium on advanced intelligent systems (ISIS) (pp. 16–21). IEEE.
22. Marino R, Scalzi S, Netto M (2011) Nested PID steering control for lane keeping in autonomous vehicles. Control Eng Pract 19(12):1459–1467
23. Yoon J, Doh J (2022) Optimal PID control for hovering stabilization of quadcopter using long short term memory. Adv Eng Inform 53:101679
24. Li JW, Chen XB, Zhang WJ (2010) Axiomatic-design-theory-based approach to modeling linear high order system dynamics. IEEE/ASME Trans Mechatron 16(2):341–350
25. Liu L, Zhang L, Pan G, Zhang S (2022) Robust yaw control of autonomous underwater vehicle based on fractional-order PID controller. Ocean Eng 257:111493
26. Erol H (2021) Stability analysis of pitch angle control of large wind turbines with fractional order PID controller. Sustainable Energy, Grids and Networks 26:100430
27. Yang, XS (2010). A new metaheuristic bat-inspired algorithm. In Nature inspired cooperative strategies for optimization (NICSO 2010) (pp. 65-74). Springer, Berlin, Heidelberg
28. Perwaiz U, Younas I, Anwar AA (2020) Many-objective BAT algorithm. PLoS ONE 15(6):e0234625
29. Lakshmanaprabu SK, Elhoseny M, Shankar K (2019) Optimal tuning of decentralized fractional order PID controllers for TITO

process using equivalent transfer function. Cogn Syst Res 58:292–303
30. Chaib L, Choucha A, Arif S (2017) Optimal design and tuning of novel fractional order PID power system stabilizer using a new metaheuristic Bat algorithm. Ain Shams Eng J 8(2):113–125
31. Fang Y, Fu W, Ding H, Fei J (2022) Modeling and neural sliding mode control of mems triaxial gyroscope. Adv Mech Eng 14(3):16878132221085876
32. Lu C, & Fei J (2016). Adaptive sliding mode control of MEMS gyroscope with prescribed performance. In: 2016 14th international workshop on variable structure systems (VSS) (pp. 65–70). IEEE.
33. Guo Y, Xu B, Zhang R (2020) Terminal sliding mode control of mems gyroscopes with finite-time learning. IEEE Transact Neural Netw Learn Syst 32(10):4490–4498
34. Rahmani M, Rahman MH, Nosonovsky M (2020) A new hybrid robust control of MEMS gyroscope. Microsyst Technol 26(3):853–860
35. Yan W, Hou S, Fang Y, Fei J (2017) Robust adaptive nonsingular terminal sliding mode control of MEMS gyroscope using fuzzy-neural-network compensator. Int J Mach Learn Cybern 8(4):1287–1299
36. Kaiser E, Kutz JN, Brunton SL (2021) Data-driven discovery of Koopman eigenfunctions for control. Mach Learn: Sci Technol 2(3):035023
37. Snyder G, & Song Z (2021) Koopman operator theory for nonlinear dynamic modeling using dynamic mode decomposition. arXiv preprint arXiv:2110.08442.
38. Malarvili S, Mageshwari S (2022) Nonlinear PID (N-PID) controller for SSSP grid connected inverter control of photovoltaic systems. Electric Power Syst Res 211:108175
39. Guo TY, Lu LS, Lin SY, Hwang C (2022) Design of maximum-stability PID controllers for LTI systems based on a stabilizing-set construction method. J Taiwan Inst Chem Eng 135:104366
40. Yan L, Webber JL, Mehbodniya A, Moorthy B, Sivamani S, Nazir S, Shabaz M (2022) Distributed optimization of heterogeneous UAV cluster PID controller based on machine learning. Comput Electr Eng 101:108059
41. Abdelouahab MS, Hamri NE (2016) The Grünwald-Letnikov fractional-order derivative with fixed memory length. Mediterr J Math 13(2):557–572
42. Yang XS (2012). Bat algorithm for multi-objective optimisation. arXiv preprint arXiv:1203.6571.
43. Sathya MR, Ansari MMT (2015) Load frequency control using Bat inspired algorithm based dual mode gain scheduling of PI controllers for interconnected power system. Int J Electr Power Energy Syst 64:365–374
44. Mitić M, Miljković Z (2015) Bio-inspired approach to learning robot motion trajectories and visual control commands. Expert Syst Appl 42(5):2624–2637